https://doi.org/10.2352/issn.2169-2629.2021.29.111

Real World Metamer Sets: Or How we Came to Love Noise

Peter Morovič, Ján Morovič, HP Inc., Sant Cugat del Valles, Spain

Abstract

It is well known that color formation acts as a noise-reducing lossy compression mechanism that results in ambiguity, known as metamerism. Surfaces that match under one set of conditions – an illuminant and observer or capture device – can mismatch under others. The phenomenon has been studied extensively in the past, leading to important results like metamer mismatch volumes, color correction, reflectance estimation and the computation of metamer sets – sets of all possible reflectances that could result in a given sensor response. However, most of these approaches have three limitations: first, they simplify the problem and make assumptions about what reflectances can look like (i.e., being smooth, natural, residing in a subspace based on some measured data), second, they deal with strict mathematical metamerism and overlook noise or precision, and third, only isolated responses are considered without taking the context of a response into account. In this paper we address these limitations by outlining an approach that allows for the robust computation of approximate unconstrained metamer sets and exact unconstrained paramer sets. The notion of spatial or relational paramer sets that take neighboring responses into account, and applications to illuminant estimation and color constancy are also briefly discussed.

Introduction

While the dimensionality of human color vision is discrete and three-dimensional, that of the stimuli it responds to can either be thought of as continuous or as sampled in a much higher-dimensional way. It is common to represent spectral power distributions or spectral reflectances at intervals of 10 nm in the range of at least 400–700 nm, which yields a 31–dimensional vector.

A direct consequence of such higher dimensionality is a many to one relationship. Under given conditions, there is a variety of spectra that differ among themselves but where all of them give rise to a single response. Such a set of all spectra that correspond to a single response is called a metamer set and characterizing it – instead of identifying a single spectrum – is the most complete answer to the question of what stimulus may have given rise to a given response. The volume of metamer sets then is an indication of the uncertainty of picking any single spectrum as the source of a response. And the same also holds when the viewer is not a human but an imaging system like a scanner or camera.

The high-dimensional nature of spectra makes their direct computation problematic, since computing boundaries in 31 or even 16 dimensional spaces (for a 20 nm sampling of 400-700 nm) is impractical. A further, and more fundamental, challenge is that metamer sets are dimensionally deficient – i.e., a set of metamers in 31D will have a dimensionality lower than 31, which yields zero volume.

Instead, the exact computation of metamer sets is constrained to a projection onto another domain – e.g., an orthogonal complement of XYZ under a given illuminant (e.g., D50 or D65), or simply multiple illuminant-observer combinations. A consequence of the difficulty of dealing with metamer sets directly in spectral terms is also the practice of computing metamer set volumes in colorimetric terms. The result is the concept of a metamer mismatch volume, where the degree of a surface's potential for metamerism is quantified by computing the volume in a colorimetric space (e.g., CIEXYZ) under a second illuminant that contains the colorimetries of reflectances that under a first illuminant are metamers. The greater the volume under the second illuminant the greater the potential for metamerism that surfaces have, which match under a first illuminant (Logvinenko *et al.*, 2014).

To counter the challenge of operating in a high-dimensional spectral space, and taking advantage of the lower-dimensional variance in natural spectra, dimensionality reduction techniques like Principal Component Analysis (PCA), Independent Component Analysis (ICA) and Neural Networks (NN) (e.g., Ramanath *et al.*, 2004) have been used. Even when natural spectra are represented in a decorrelated basis, obtained, e.g., using PCS, the need for around 8 bases for representing their variance is not uncommon (e.g., Krinov, 1947; Vrhel *et al.*, 1994). While such an approach is beneficial when studying the spectra of natural surfaces, it poses problems when applied to some scenarios, such as spectral power distributions under LED lighting (for which, e.g., Finlayson *et al.* (2014) provide an elegant solution by using the LED spectra as basis functions and convex combinations for modelling the LED output's peak wavelength shift with intensity).

Dimensionality reduction also significantly underpredicts metamer mismatch volumes, as was shown recently by Mackiewicz *et al.* (2019), who presented a solution to metamer set computation that avoids such reduction. It works by leveraging an approach to efficiently computing the spectra delimiting the Object Color Solid (OCS) (Schödinger, 1920), i.e., the convex hull of all possible responses for a given illuminant-observer combination. This is done using a spherical sampling that yields spectra on the OCS boundary in a sampling of all spherical directions. The same method is then used for a given response, where reflectances are maximized in spherical spectral directions.

An approach that side-steps the dimensional ill-posedness of exact metamer set computation is the move from metamer sets (i.e., a strict correspondence between multiple spectra and a single response) to paramer sets, which are sets of spectra whose responses are within some, usually narrow, neighborhood in a space representing responses (e.g., CIE XYZ or camera RGB values). An early motivation for the introduction of tolerances instead of an exact match was to mimic the human visual system's response where physical changes below a certain threshold – the just noticeable difference (JND) – do not result in a change in its sensory response (e.g., Samadzadegan and Urban, 2015). Such response relaxation also allows for variation to be introduced on the spectral side that results in well-posed, fully-dimensional spectra.

There is another motivation for using paramer sets, beyond taking into account JNDs, which is the presence of noise in all measured/captured data. Whether it be image capture using cameras or scanners or the measurement of reflectance or colorimetry, noise is always present. This begs the question of what the meaning of a metamer set is beyond the purely theoretical. In practice it is never

a response for which a corresponding set of possible spectra is sought, but a distribution of responses due to capture or measurement noise whose paramer set needs to be characterized. Working with paramer sets where the response range is the result of noise leads to more reliable predictions of response-spectrum correspondence. This, in turn, can improve the accuracy and robustness of estimating captured light properties.

In this paper we present an exploration of various aspects of moving from operating on metamer sets, which is unnecessarily hard and does not correspond to real situations, to paramer sets, where as much information as is available is used (e.g., multiple measurements/captures, spatial context, …) to make estimates and predictions that fit practical applications more closely. An example of using paramer sets in conjunction with spatial information is Samadzadegan and Urban's 2015 paramer-mismatch-based spectral gamut mapping (PMSGM) where paramer sets projected into colorimetry under multiple illuminants and for spatial neighborhoods are intersected to obtain printed colors that optimize color matching for those illuminants and do so in a spatially consistent way.

Unconstrained Metamer and Paramer Sets

Computing surface metamer sets means computing the set of all possible reflectances that, given an illuminant and an observer or camera sensor, match a given response. This means inverting the color formation equations. Let us assume the Mondrian world of flat, Lambertian surfaces where color formation follows the well-known equation:

$$\boldsymbol{x} = \boldsymbol{r} * (\boldsymbol{l} \bullet \boldsymbol{S}^T) \tag{1}$$

where $\boldsymbol{r}$ is the reflectance vector, $\boldsymbol{l}$ the illuminant (light source) vector and $\boldsymbol{S}$ the sensor sensitivities, with • denoting the vector dot-product, and $\boldsymbol{x}$ the sensor response.

Both $\boldsymbol{r}$ and $\boldsymbol{l}$ are $1xn$ vectors (where n is the spectral sampling, e.g., 31 or 16) and $\boldsymbol{S}$ is an mxn matrix where m is the number of sensors resulting in $\boldsymbol{x}$ being a 1xm vector of sensor responses (e.g., 3 for an RGB camera where $\boldsymbol{x}$ = RGB or the CIE color-matching functions where $\boldsymbol{x}$ = XYZ). The dot-product ($\boldsymbol{l} \bullet \boldsymbol{S}^T$) is also known as the mxn "lighting matrix" and often denoted as $\boldsymbol{A}$ (Maloney and Wandell, 1986).

As is well known, the mismatch between m and n implies that Eq. (1) is under-determined in terms of reflectance $\boldsymbol{r}$, meaning that if all else is constant ($\boldsymbol{x}$, $\boldsymbol{l}$, $\boldsymbol{S}$), there is no unique solution $\boldsymbol{r}$ to the equation and, in fact, the solution is in an n-m dimensional subspace, and therefore has n-m degrees of freedom. The solution space can be shown to be a convex subset and to have infinitely many solutions (Morovič, 2002). As a corollary, as m approaches n, the degrees of freedom diminish as does the under-determined nature of Eq. (1). The more sensors one has available in $\boldsymbol{S}$, the lower the degree of metamerism. In the limit, when $m = n$ and spectral sampling matches the number of sensors (assuming they are decorrelated), there is a unique solution for $\boldsymbol{r}$.

Substantial advances have been made in the literature to narrow down the solution space of $\boldsymbol{r}$, inspired by an important intuition about reflectances: that they are not arbitrary vectors and typically exhibit specific properties. It is then possible to dimensionally reduce the reflectance space using principal component analysis (PCA) or characteristic vector analysis (CVA). If we assume that all reflectances can be written as linear sums of some pre-defined set of p basis functions $\boldsymbol{B}$:

$$\boldsymbol{r} = \boldsymbol{w} * \boldsymbol{B} \tag{2}$$

then Eq. (1) becomes:

$$\boldsymbol{x} = \boldsymbol{w} * \boldsymbol{B} * (\boldsymbol{l} \bullet \boldsymbol{S}^T) \tag{3}$$

where $\boldsymbol{B}$ is a linear model basis (Maloney, 1986) that defines a lower-dimensional, decorrelated coordinate system that represents reflectance space. Inverting Eq. (3) then becomes solving for $\boldsymbol{w}$ where $\boldsymbol{w}$ is a $1xp$ vector with $p \ll n$. Both the strengths and pitfalls of such linear model bases come from being tailored to a particular data set. This can be advantageous and enable tuning a solution to a particular ecosystem, but it also means a threat to generality.

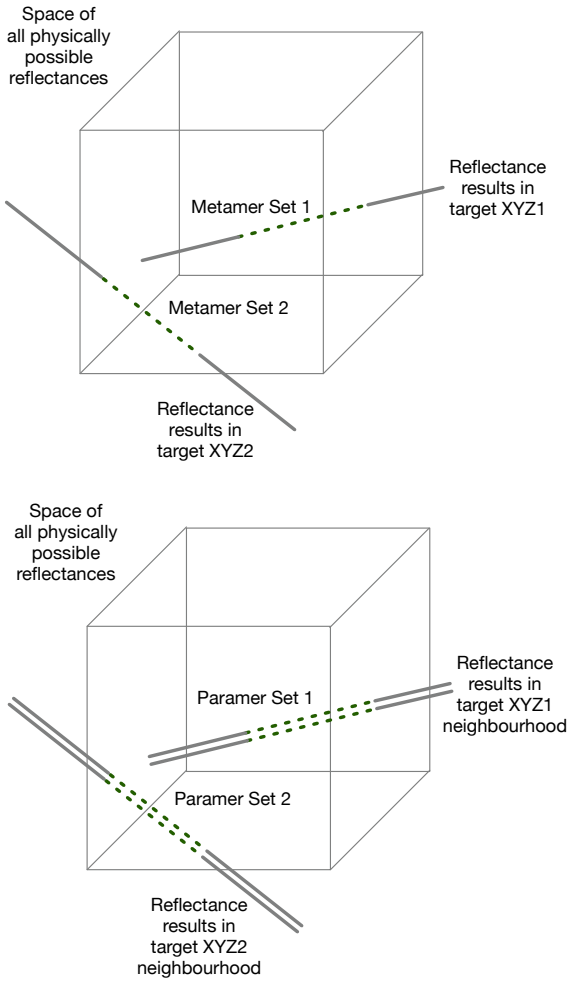

Figure 1: Illustration of degenerate metamer set – where the line has no volume (top) vs full-dimensional paramer set – where the intersection has volume (bottom).

Turning back to Eq. (1), constraints on reflectances that hold for all physically possible surface reflectances can still be formulated. Excluding materials such as fluorescents, quantum dots and other photoluminescent effects that allow for down-shifting incident energy (i.e., emitting energy at a wavelength different from than at which it was absorbed), all reflectances have to follow:

$$\mathbf{0} \leq \boldsymbol{r} \leq \boldsymbol{u} \tag{4}$$

Typically, the inequalities of Eq. (4) would be written as $\boldsymbol{r} \leq \mathbf{1}$ but there is no need to fix the upper bound $\boldsymbol{u}$ to $\boldsymbol{1}$, although it will often be close to 1 (e.g., optical brighteners of common print substrates yield values above 1). Nevertheless, it is useful to consider that reflectances are not arbitrary vectors (Morovič, 2002).

Given the above conditions, inverting Eq. (1), with the added constraints of Eq. (4) amounts to intersecting an *n-m* dimensional hyperplane (Eq. (1)) with an *n*-dimensional hypercube (Eq. (4)). While this is a tractable problem, the solution is degenerate and often fragile to compute using standard convex hull solutions – i.e., while reflectances are in *n*-dimensional space, the solution to the metamer set problem resides in an *n-m* dimensional subspace and therefore has no volume. Fig. 1 (top) illustrates this schematically: the solution space of all reflectances (hypercube) is represented by a 3D cube and the sub-space defined by color formation (i.e., the reflectances that match a given response) is represented by a line in 3D (a degenerate, not fully-dimensional object), with their intersection shown as a line segment.

Robust Approximate Metamer Set Computation

One way to overcome such computational fragility is to break down the convex hull computation and compute an approximation, without assuming that the resulting hull will be fully–dimensional. The approach we describe below enables to do this robustly, albeit not efficiently, and in a way that results in an under-estimate of the true metamer set.

The basic intuition behind this method is to consider the fact that the convex hull can be described in a number of ways: as linear inequalities (delimiting the convex region) or as a set (strictly speaking the smallest set) of vertices that describe the convex region. The definition of the metamer set is given as the intersection of the inequalities in Eq. (4) and the strict equality constraint in Eq. (3), while the solution(s) $\boldsymbol{r}$ reside in an n-dimensional space forming an *n-m* dimensional convex polytope. If we can compute the extreme vertices of this convex object then the full solution would lie in a sub-space of n-dimensional space and would therefore be degenerate (i.e., would have no volume). An alternative approach is to consider this problem in each dimension and all its dimension-combinations one by one, resulting in a set of points that will be a convex region and will under-estimate the true metamer set.

Since the extremes of the convex region are the smallest and the largest values, we can formulate this problem as follows.

First, we define the set of all combinations from 1 to n as the set of vectors $\boldsymbol{i}$ that contain all combinations of *1, 2, 3, …n* out of *n* – this would correspond to, e.g., wavelength 1 (e.g., 400 nm), 2 (e.g., 410 nm), etc., followed by wavelength 1 and 2 (e.g., 400, 410 nm), 1 and 3, etc., all the way to all wavelengths 1 to n. Let us denote this set as $\boldsymbol{C}$ and define it as:

$$\boldsymbol{C}: \{\boldsymbol{i}, \boldsymbol{i} \in \binom{\boldsymbol{n}}{\boldsymbol{j}} : \boldsymbol{j} \in \{\mathbf{1}, \ldots, \boldsymbol{n}\}\} \tag{5}$$

Then, for each combination of 1 to n wavelengths from C, we compute the minimization and maximization problem:

$$\boldsymbol{x} = \boldsymbol{r} * (\boldsymbol{l} \bullet \boldsymbol{S}^T) \; st. \mathbf{0} \leq \boldsymbol{r} \leq \boldsymbol{u}$$

$$\boldsymbol{min}\, \boldsymbol{r}_i \; \forall \, \boldsymbol{i} \in \boldsymbol{C}$$

$$\boldsymbol{max}\, \boldsymbol{r}_i \; \forall \, \boldsymbol{i} \in \boldsymbol{C} \tag{6}$$

In other words, for each dimension and each dimension combination we evaluate two optimizations, a minimization and a maximization – to obtain the partial extremes of the true convex hull. Given that this computation is done per dimension and dimensional combination, it results in a large number of combinations – e.g., for 16 spectral samples (400 to 700 at 20 nm steps) there are 65536 optimizations. Since the constraints are linear inequalities and the optimization is a linear objective function, this computation can be formulated using Linear Programming (Chvatal, 1983). Here the indices in C serve to determine the value of the objective function (e.g., 1 for minimizing and -1 for maximizing) – and takes about 15s per colorimetry on a common desktop computer. While this can be practical and useful, since reflectances computed in this way are strict metamers, the result is an approximation and an under-estimate of the true metamer set that still suffers from degenerate dimensionality.

Unconstrained Paramer Set Computation

To address this shortcoming of the exact approach, we introduce the notion of noise into the equation – departing from the strict mathematical definition of metamerism. In the literature this is sometimes referred to as *paramerism* or *paramer sets*, where instead of a strict, exact equality, a near-match is sought. As described earlier, not only does considering a near-match make the problem more real-world-like, it also has important consequences for the solution.

The simplest way to consider a near-match or to account for some kinds of noise is by relaxing Eq. (1) as follows:

$$\boldsymbol{x_L} \geq \boldsymbol{r} * (\boldsymbol{l} \bullet \boldsymbol{S}^T) \wedge \boldsymbol{x_U} \leq \boldsymbol{r} * (\boldsymbol{l} \bullet \boldsymbol{S}^T) \tag{7}$$

where instead of a single target response $\boldsymbol{x}$, a lower ($\boldsymbol{x_L}$) and upper ($\boldsymbol{x_U}$) bounds are used. Reflectances that are a solution to Eq. (7) will then result in responses that reside inside the hypercube described by these two extremes. Taking Eq. (7) and combining it with Eq. (4) then results in a set of linear inequalities that jointly define a convex volume in the reflectance space. Eq. (4) are *2n* inequalities while Eq. (7) are 6 inequalities, written together in canonical form ($\boldsymbol{Ax} \leq \boldsymbol{b}$) as follows:

$$\boldsymbol{r} \leq \boldsymbol{u}$$

$$-\boldsymbol{r} \leq \mathbf{0}$$

$$(\boldsymbol{l} \bullet \boldsymbol{S}) * \boldsymbol{r} \leq \boldsymbol{x_U}$$

$$-(\boldsymbol{l} \bullet \boldsymbol{S}) * \boldsymbol{r} \leq -\boldsymbol{x_L} \tag{8}$$

For a given $\boldsymbol{x_U}$, $\boldsymbol{x_L}$ and $\boldsymbol{l}$, $\boldsymbol{S}$, the set of inequalities in Eq. (8) therefore describes a halfplane intersection, or convex hull computation, that results in a non-degenerate *n*-dimensional subspace and can be computed using common convex hull libraries such as qhull (Barber *et al.*, 1996).

While the mechanism to introduce a range of possible responses above is a very simple one – an enclosing hypercube (or cube for tristimulus or RGB responses). The principle can be generalized to allow for arbitrary convex sub-spaces. E.g., if noise is defined as a unit-sphere in CIE L*a*b* – e.g. a sphere where all surface points are at most 1 DE76 from all other points on or in the sphere – by means of discretizing the sphere in L*a*b* (approximating it with a polyhedron), converting the result to XYZ and computing the convex hull in the form of linear inequalities that

enclose it in XYZ, results in constraint that can directly be used in Eq. (8). Instead of the upper and lower bound $\boldsymbol{x_U}$, $\boldsymbol{x_L}$ a set of inequalities – again in the canonical form ($\boldsymbol{Ax} \leq \boldsymbol{b}$) that delimit the target region, representing an arbitrary geometric representation of noise (expressed in XYZ) are then used:

$$\boldsymbol{A} * (\boldsymbol{l} \bullet \boldsymbol{S}) * \boldsymbol{r} \leq \boldsymbol{b} \tag{9}$$

To conclude, what we have presented here are two methods: one that is approximate but robust and uses the strict metamerism definition (via linear programming) and a second one that relaxes the strict definition and computes paramer sets exactly and directly. Fig. 1 (top) illustrates the above approach schematically and shows that if instead of strict equality, a small range of responses is used in the computation of a paramer set, the resulting solution space is not degenerate and has volume.

Results and Examples

In order to explore the previously defined computations, this section shows examples for some sample configurations. Fig. 2 first shows a real example of this computation using CIE illuminant D50 as $\boldsymbol{l}$ and the CIE 1931 color matching functions as the reference illuminant and observer as $\boldsymbol{S}$, with an upper bound for reflectance values of $\boldsymbol{u}$=1 and for an XYZ of [17.1, 22.5, 10.6] – computed based on a green sample from a set of 426 Munsell chips – with a tolerance of 0.5 in XYZ terms, resulting in $\boldsymbol{x_L}$ = [16.6, 22.0, 10.1] and $\boldsymbol{x_U}$ = [17.6, 23.0, 11.1], the set of reflectances that map to this cube in XYZ are shown in the figure as the extreme vertices of the convex hull computation, mapped to XYZ to confirm that they indeed map to the cube defined by the tolerances.

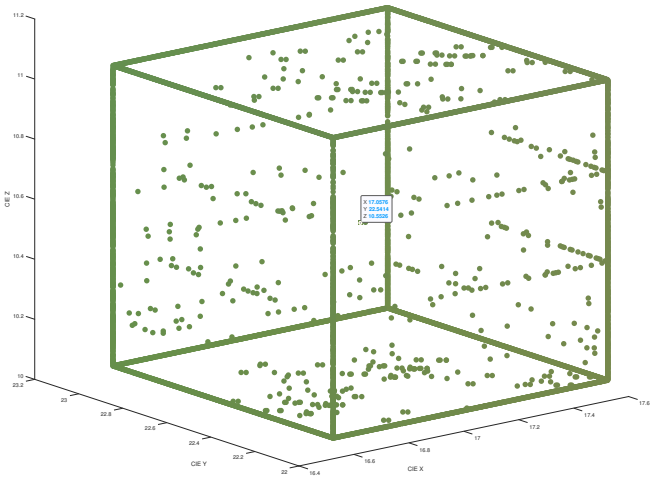

Figure 2: Paramer set reflectances projected onto XYZs under reference conditions (XYZ, D50) with 0.5 +/- in each of X, Y, Z. Note the scale of the axes that show the above paramer set cube to be of side 1 in each X, Y, Z. The labeled mid-point shows the exact XYZ.

Fig. 3 then also shows the same reflectances that in Fig. 2 are projected onto the XYZ D50 space (he reference set-up), as reflectances. Here a 16 spectral sample representation was used, from 400 to 700 nm at 20 nm steps. As can be seen, the reflectances (plotted in green) contain high frequency components (i.e., they alternate between extremes liberally and frequently, rather than being smoothly varying), however they are also clearly not arbitrary and have, e.g., concentrated variability in the 500 to 650 nm range. For comparison, an 8D linear model basis solution is also plotted (grey dashed lines) as well as a reference (measured) reflectance of the Munsell chip (shown in black) and normalized XYZ curves, that help understand the intuition of where more variation (e.g., the 500 to 600nm) and where less (e.g. past 600nm or below 420nm) are to be expected. Note here is that the linear model basis – as expected – enables similar solutions to those of the reference reflectance (which was part of the basis computation), while the unconstrained solution also contains these reflectances (by definition) but represents a much larger variety of possible reflectance curvesm even 'unnatural' ones.

This figure highlights the earlier point that using a linear model basis in a closed ecosystem where reflectances are known and where the expectation is to deal with reflectances of similar kinds can work well, however it does not allow for arbitrary reflectances and clearly results in significantly reduced spectral variety. Conversely, the unconstrained set clearly results in reflectances that are uncommon, contain unusual high frequencies and are unlikely to be natural (in a loose sense of the word), but is therefore more general and contains all possible reflectances (natural or synthetic) that could potentially result in the target colorimetry neighborhood.

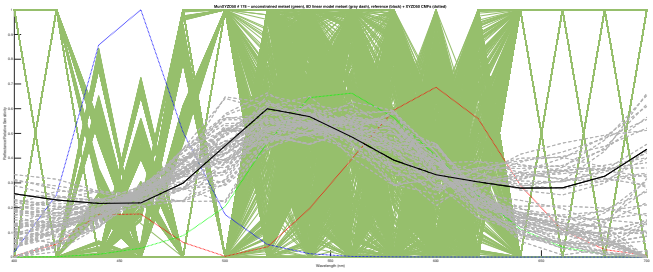

Figure 3: Paramer set, physically possible reflectances (green), constrained, linear model 8D basis reflectances (gray dashed), reference reflectance (Munsell 178). The XYZ D50 color matching functions are shown for reference.

While Fig. 3 shows the nature of reflectances that the unconstrained method results in and intuitively implies a larger volume, we can also compute and illustrate this by projecting the metamer or paramer sets onto a different set-up, e.g., by changing from CIE illuminant D50 to A as is commonly done in metamer mismatch volume studies. Fig. 4 shows the convex polytopes in XYZ (for illuminant A) for three cases: the 8D linear model basis (darkest volume), the unconstrained LP-based approximate solution to the exact metamer set (lighter volume) and the direct convex hull paramer set solution (with tolerance 0.5 in XYZ as before) – where the darkest and lightest volumes correspond to the reflectances plotted as grey lines and green lines in Fig. 3 before.

Next, we apply this analysis to the full MacBeth ColorChecker chart. Fig. 5 shows the 24 colorimetries of this chart using a tolerance of ±0.5 and CIE D50 and 1931 XYZ reference conditions, as before. The target colorimeters are cubes around the target XYZ (with an edge of 1) are plotted in an XZ 2D projection of XYZ space.

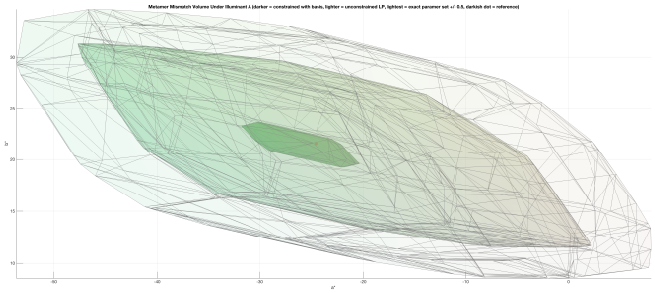

Figure 4: Metamer mismatch volumes: darkest (8D linear model basis), lighter (unconstrained LP solution), lightest (exact solution, paramer set with +/- 0.5 in XYZ).

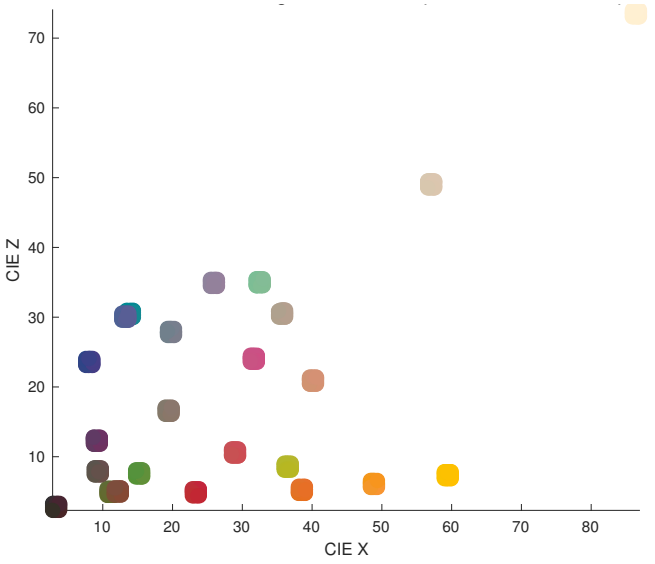

Figure 5: Target XYZ colorimetries of the 24 Macbeth colorchecker chart data set, including tolerance of ±0.5 (cubes in XYZ with side 1).

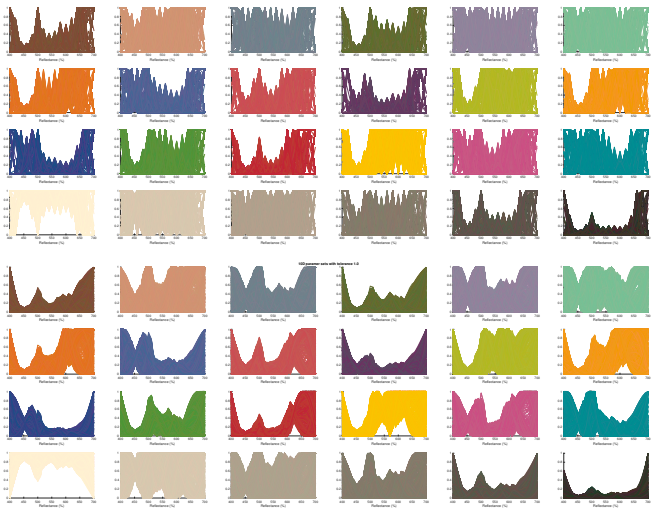

Figure 6: Paramer set reflectances corresponding to XYZ cubes in Figure 4 that match the 24 Macbeth colorchecker chart data set with a tolerance of ±0.5 (cubes in XYZ with side 1) – top, and strict metamer sets in a 10D linear model basis (matching the paramer set centres) - bottom.

Fig. 6 (top) then shows the resulting reflectances (a subset of 1000 of the extreme reflectances is plotted in each case for illustrative purposes). Again, like in Fig. 3, the large variability and high frequency of the unconstrained samples is clearly visible. Fig 6. (bottom) then also plots the corresponding, but exact metamer set reflectances using a 10D linear model basis which, as expected show smoother behavior compared to the full, unconstrained paramer sets. Note that, to obtain solutions for all 24 patches below, the metamer set computation that relies on a linear model basis had to use 10 dimensions in this case. Fewer dimensions would have left some of the patches without solutions. Part of the challenge with linear model bases is precisely the uncertainty about the exact dimensionality of a data set – another form of fragility of this formulation (exact metamerism, linear model basis).

Finally, Fig. 7, shows the mismatch volumes of the paramer reflectances from Fig. 6 (top) under illuminant A, shown here in CIE L*a*b* space.

One important aspect of the unconstrainted, fully–dimensional and therefore spectrally–volumetric computation of paramer sets is that volumes can be computed independently of a change of conditions and natively in reflectance space. Previous studies were constrained to perform these computations in a second projected space, e.g., as shown above, by changing from CIE D50 to CIE A. However, since the present solution computes paramer sets with spectral volume in their own right, we can evaluate them as such. Fig. 8 illustrates this – and can be compared against Fig. 5 – here we see the magnitude of the paramer volumes plotted at the locations of the target XYZ centres.

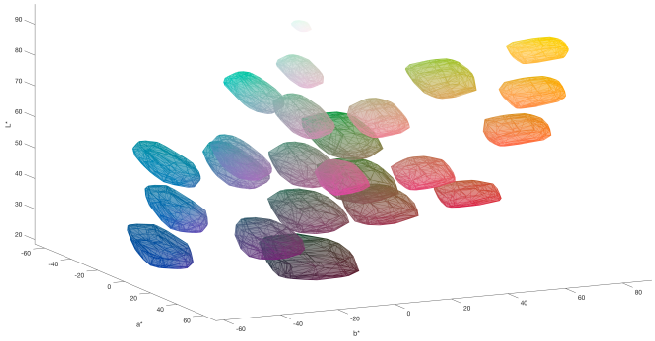

Figure 7: Paramer mismatch volumes shown in CIE Lab space as projected to CIE illuminant A, corresponding to reflectances in Fig. 5 that result in tristimulus values in XYZ cubes in Figure 4 that match the 24 Macbeth colorchecker chart data set with a tolerance of ±0.5 (cubes in XYZ with side 1).

With the introduction of a tolerance in the computation of paramer sets, the choice of this value becomes important. As mentioned in the introduction, it can be directly related to JNDs or noise, such as measurement or repeatability noise – both in magnitude and geometry (Clouet, 2020). For example, typical spectrophotometers can have a measurement repeatability of between 0.01 to 0.1 ΔE2000 – meaning that measuring the same surface multiple times. This means that the same surface can result in tristimulus values that vary within a neighborhood of this magnitude and for all intents and purposes can be considered identical, even if not mathematically so. In colorimeters and cameras the measurement or capture repeatability can be even higher.

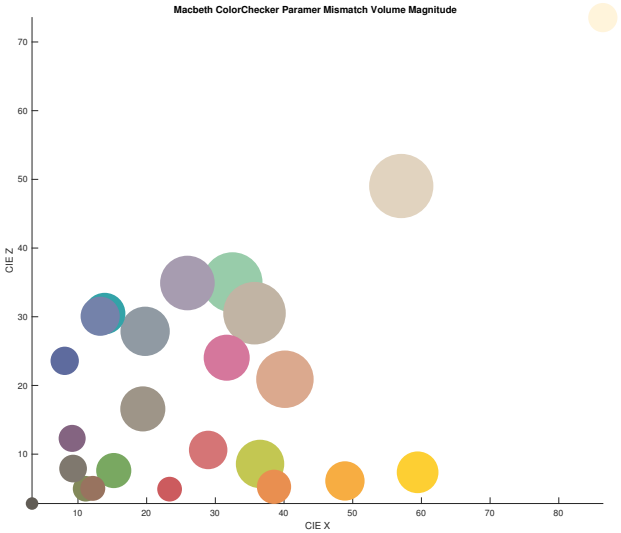

Figure 8: Paramer mismatch volumes shown in XYZ space (XZ projection), corresponding to reflectances in Fig. 5 that result in tristimulus values in XYZ cubes in Figure 4 that match the 24 Macbeth colorchecker chart data set with a tolerance of ±0.5 (cubes in XYZ with side 1).

Both the magnitude and geometry of noise or tolerance will clearly impact paramer set volumes and Fig. 9 illustrates this difference for two values (maintaining the set-up used so far: CIE D50, 1931 color matching functions), a tolerance of ±0.05 and a tolerance of ±0.95, again in CIE XYZ space. As expected, the smaller the tolerance (e.g., 0.05) the smaller the volume (as shown in this projection to CIE A). On a more qualitative and intuitive note, the larger the tolerance (e.g. 0.95) the more "bulged out" the mismatch volumes. While several aspects affect the shape and volume of mismatch volumes (e.g., the source and destination projection spaces such as CIE D50 vs CIE A), again, intuitively, the larger the tolerance the further a departure from the *n-m* dimensional subspace solution of a strict metamer set.

Fig. 9 shows the impact of the tolerance value (for a cube neighborhood in XYZ) in qualitative terms for two extreme values – 0.05 and 0.95 – while Fig. 10 shows the same relationship in quantitative terms for intermediate values. Here, paramer sets for the same set-up (Macbeth ColorChecker chart colorimetries as anchors, CIE D50, 1931 color matching functions) and tolerances from 0.05 to 0.95 in 0.1 steps in XYZ are computed and a comparison between traditional metamer mismatch volumes (as computed by projecting to a tristimulus space by changing the illuminant from CIE D50 to CIE A) vs the direct spectral volume of paramer mismatch volumes is shown. First, it can be observed that the larger the tolerance the larger the volumes – this is as expected and simply means that the wider the allowed colorimetric correspondence the more reflectances correspond and this is true in spectral volume terms as in illuminant-mismatch volume terms. However, what can also be seen is that the relationship between spectral volume and illuminant-mismatch volume is not straightforward and does not seem to follow a simple relationship, while being highly correlated.

In the final paper we will share a more detailed analysis of this relationship and explore how it varies for other changes in illuminant.

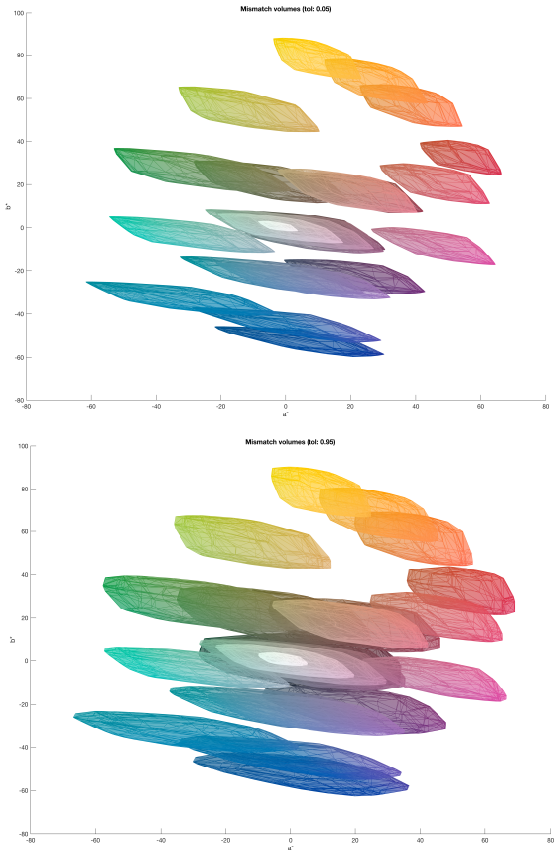

*Figure 9: Paramer mismatch volumes shown in CIE Lab space (a*b* projection), corresponding to the 24 Macbeth colorchecker chart data set with a tolerance of ±0.05 (top) and ±0.95 (bottom).*

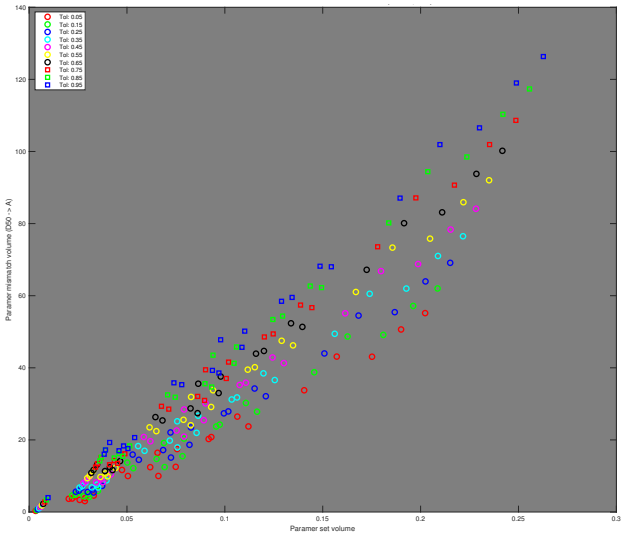

Figure 10: Paramer set mismatch spectral-volumes vs projected tristimulus volumes for 10 paramer tolerances centered around the 24 Macbeth Colorchecker chart colorimetries (CIE D50, 1931). The markers indicate tolerance levels (red circle = ±0.05, blue square ±0.95).

Discussion and conclusions

This paper revisits the topic of metamerism, with a particular focus on its relation to real-world conditions and computational robustness. First, a method to overcome the computational fragility of exact metamer sets was presented via an approximate approach using linear programming. Next, a generalization of the metamer set, allowing for tolerances to the exact tristimulus target and resulting in a paramer set, were shown to allow for a direct and exact computation, while at the same time being a better mechanism in real-world situations where exact mathematical matches are never the case due to measurement and repeatability noise and the human visual system's or any imaging system's discrete response to stimulus change.

While better real-world representation and computational robustness are clear benefits, the purpose of this paper was also to emphasize the importance of taking uncertainty into account and to show how doing so is ultimately also advantageous.

The introduction of this approach and the formulation of a solution also open up the possibility of computing and operating with paramer set intersections. In exact metamer sets, intersections are fragile like the direct single metamer set computation itself (since a metamer set is a degenerate *n-m* dimensional hyperplane without volume). Instead, using the paramer set definition and computation shown here allows for a robust solution that can also be parametrized by tolerance level. E.g., what is the tolerance level at which two paramer sets intersect? Conversely, which paramer sets intersect at a given tolerance level?

There are many applications of paramer set intersections that will be explored in the future, including:

Spatial paramer sets – i.e., computing paramer sets that take spatially–neighboring responses into account. In most real-world cases, responses are not isolated data points but are embedded in context, such as neighboring pixels in a digital image. Using this context is another way to help deal with and benefit from uncertainty and noise, and is likely to result in more robust computation and potentially better color correction and camera characterization.

Illuminant estimation – varying the reference conditions for which paramer sets are computed and evaluating their volume could lead to intuitions on the likelihood of illuminants or materials – the larger the volumes the more likely an illuminant.

Material and illuminant edges – computing intersections of paramer sets in an image, could help distinguish material (e.g., surface reflectance) vs illuminant (e.g., light source spectral power distribution) changes and therefore help identify where in an image a change in illuminant or material (or both) occur. With a known illuminant, instead, material edges can be identified by evaluating paramer set intersections – the smaller the intersections the more likely a material edge.

Acknowledgements

The authors would like to thank their colleagues Alan Lobban, Elizabeth Zapata and Konstantinos Kontonikolas at HP Inc. for their support.

References

[1] Barber C.B., Dobkin D.P., Huhdanpaa H.T. (1996) *The Quickhull algorithm for convex hulls*, ACM Trans. on Mathematical Software, **22**(4):469-483.

[2] Clouet A., Vaillant J., Alleysson D. (2020) *The Geometry of Noise in Color and Spectral Image Sensors*. Sensors (Basel). **20**(16):4487. doi: 10.3390/s20164487. PMID: 32796625; PMCID: PMC7471994.

[3] Chvatal V. (1983) *Linear Programming*. W.H. Freeman. ISBN 978-0-7167-1587-0.

[4] Finlayson G., Mackiewicz M., Hurlbert A., Pearce B., Crichton S. (2014) *On calculating metamer sets for spectrally tunable LED illuminators*, J. Opt. Soc. Am. A, **31**, 1577-1587.

[5] Finlayson G. D., Morovic P., *Metamer sets*, J. Opt. Soc. Am. A **22**, 810-819 (2005)

[6] Krinov E. L. (1947) *Spectral Reflectance Properties of Natural Formations*, Proceedings of the Academy of Sciences of the USSR.

[7] Logvinenko A. D., Funt B., & Godau C. (2014) *Metamer Mismatching*, IEEE Trans. on Image Processing, **23**(1), 34-43.

[8] Logvinenko A. D., Funt B., Mirzaei H., Tokunaga R. (2015) *Rethinking Colour Constancy*. PLoS ONE, **10**(9): e0135029. doi:10.1371/journal. pone.0135029

[9] Mackiewicz M., Rivertz H. J., Finlayson G. (2019) *Spherical sampling methods for the calculation of metamer mismatch volumes*, J. Opt. Soc. Am. A, **36**, 96-104.

[10] Maloney L.T. (1986) *Evaluation of linear models of sur- face spectral reflectance with small numbers of parameters*. J. Opt. Soc. Am. A, **3**(10):1673– 1683.

[11] Maloney L. T., Wandell B. A. (1986) *Color constancy: a method for recovering surface spectral reflectance*, J. Opt. Soc. Am. A, **3**, 29–33.

[12] Morovic P. (2002) *Metamer Sets*. PhD. Thesis, University of East Anglia, School of Computing Sciences, Norwich (UK)

[13] Ramanath R., Kuehni R. G., Snyder W. E., Hinks D. (2004) *Spectral Spaces and Color Spaces*, Color Research & Application, **29**(1), 29–37.

[14] Schrödinger E. (1920) *Theorie der Pigmente von größter Leuchtkraft*, Annalen der Physik, **367**, 603–622.

[15] Vrhel M. J., Gershon R., Iwan L. S. (1994) *Measurement and analysis of object reflectance spectra*, Color Research and Application, **19**(1), 4–9.

Author Biography

Peter Morovič received his Ph.D. in computer science from the University of East Anglia (UK) in 2002 and holds a B.Sc. in theoretical computer science from Comenius University (Slovakia). He has been a senior color and imaging scientist at HP Inc. since 2007, has published 60+ scientific articles and has 150+ US patents filed (116 granted) to date. His interests include 2D/3D image processing, color vision, computational photography, computational geometry. His Erdős number is 4.

Ján Morovič received his Ph.D. in color science from the University of Derby (UK) in 1998, where he then worked as a lecturer. Since 2003 he has been at Hewlett-Packard in Barcelona as a senior color scientist and later master technologist. He has also served as the director of CIE Division 8 on Image Technology and Wiley and Sons have published his 'Color Gamut Mapping' book. He is the author of over 100 papers and has filed 150+ US patents (119 granted).